JETIR.ORG ISSN: 2349-5162 | ESTD Year : 2014 | Monthly Issue
JOURNAL OF EMERGING TECHNOLOGIES AND INNOVATIVE RESEARCH (JETIR)
An International Scholarly Open Access, Peer-reviewed, Refereed Journal

Effect of Unusual Shape of Stenosis on Blood Flow in Stenosed Artery

Sangeeta

(Department of Mathematics, Maharshi Dayanand University, Rohtak)

Abstract

The current mathematical model examined blood behavior in arteries with unique geometries. Studying blood flow through a strange shape with a magnetic field is the primary goal of this investigation. The mathematical model utilized for the evaluation employs the parameter variation method to solve coupled partial differential equations. The main conclusions are graphically displayed and examined for different values of the dimensionless parameters. In order to study the general behavior of blood flow patterns, the velocity profile for a number of recently developing characteristics is shown. The newest studies are beneficial for biologically treating different cardiovascular ailments.

Keywords: *Stenosis artery, Magnetic field, Heat transfer, Bessel function, Blood flow*

Introduction

The blood channels known as arteries carry blood from the heart to every region of the body (lungs, tissues, brain etc.). The buildup of plaque on the artery walls, which narrows the flow region and causes the disease atherosclerosis or stenosis, is one of the obstacles that frequently occur in the arteries during blood flow. Stenosis hardens and narrows the blood vessels over time, reducing the amount of oxygenated blood that reaches the organs and other parts of the body and increasing the risk of serious problems like heart attack, stroke, and even death. Researchers have investigated the flow behaviour and rheology of blood both theoretically and experimentally to infer the developments in the diagnosis and treatment of vascular disorders after realizing the significance of hydrodynamic parameters in the development of heart diseases [1-10].

Prasad et al. [3] used a mathematical model for steady flow in two dimensions and considered hematocrit in their study, assuming the stenosed arterial segment tapered. Manisha and kumar [22] investigated an analytical mathematical model of a two-layered symmetric stenosed artery with integrative heat and mass transfer effects through a porous medium. Majeed et al. [27] proposed a fractional model of MHD blood flow with magnetic particles. A simplification of the problem used the Caputo time-fractional derivative and obtained a solution using the Finite Hankel and Laplace transform. They found that the motion of the blood and magnetic particles is decelerated when the magnetic parameter and the particle mass parameter are increased.

The behavior of fluid and the type of (pulsatile) flow are just two of the hidden properties of blood rheology that have been revealed via investigations of many mathematical models over the years [11-17]. Numerous studies have found that blood vessels exhibit pulsing flow behavior, and these oscillations are continuously dampened. Because it alters the flow pattern, blood artery-related disease plays a crucial role in hemodynamics by causing changes in the arteries by wall pressure and wall shear stress [8-17]. Kumar and Kumar [21] investigated model of the elliptical stenosed artery with the magnetic field, heat source and chemical reaction.

Abumandour et al. [23] improved analytical implementation of the interaction effect of slip and thermal conditions on particle fluid suspensions along vertical stenotic arterioles with or without magnetic fields and porosity. The influences of Soret and Dufour have been investigated in the bloodstream through a tapered porous stenosed artery by Sharma et al. [30]. They found that the magnetic field keeps on slowing the blood flow. Awrejcewicz et al. [24] formulated a theoretical model of the blood flow in arteries under body acceleration and the magnetic fields presence. Poonam et al. [29] discussed a computational mathematical model with nanoparticle transport in an aneurysmal and stenosed curved artery along mass and heat transfer factors. They observed the remarkable impact of hybrid nanoparticles in the presence of radiation and chemical reaction on heat mass transfer, arterial curvature on flow velocity and wall shear stress patterns. Padma et al. [28] analysis of a mathematical model of Jeffrey fluid in the tapered porous artery plays a vital role in bridge lacuna.

In the current work, magnetic field parameters are used to examine a fluid model in an abnormal stenosed artery. The study was carried out using appropriate analytical techniques. Finding the flow rate, axial velocity, and shear stress in a particular circumstance is made easier with the aid of this methodology.

Mathematical Formulation

The current two-phase model of blood circulation through the abnormal stenosed artery is pulsating, incompressible, and unstable. The viscosity and geometry of the anomalous artery are defined as two separate layers (core and plasma) as $\bar{\mu}(\bar{r}) = \bar{\mu}_c$ for core layer and $\bar{\mu}(\bar{r}) = \bar{\mu}_p$ for plasma layer

$$\bar{R}_c(\bar{z}) = \begin{cases} \beta\,\bar{R}_0 - \bar{\delta}_s\, e^{-\frac{m^2}{\bar{R}_0^2}[\bar{z}-\bar{d}-\bar{L}_0/2]^2} & ;\ \bar{d} \le \bar{z} \le \bar{d} + \bar{L}_0 \\ \beta\,\bar{R}_0 & ;\ otherwise \end{cases}$$

$$\bar{R}_c(\bar{z}) = \begin{cases} \bar{R}_0 - \bar{\delta}_s\, e^{-\frac{m^2}{\bar{R}_0^2}[\bar{z}-\bar{d}-\bar{L}_0/2]^2} & ;\ \bar{d} \le \bar{z} \le \bar{d} + \bar{L}_0 \\ \bar{R}_0 & ;\ otherwise \end{cases}$$

Where $\bar{L}_0$, $\bar{\delta}_s$, m, $\bar{R}_0$, β, are represented constriction length, maximum depth of the constriction, shape parameter, normal artery, ratio of core and normal artery

The modeling equations of the current investigation for core and plasma layers [21, 22, 23, 30] are as

$$\bar{\rho}_c\,\frac{\partial \bar{u}_c}{\partial \bar{t}} = -\frac{\partial \bar{p}_c}{\partial \bar{z}} + \bar{\mu}_c\left(\frac{\partial^2 \bar{u}_c}{\partial \bar{r}^2} + \frac{1}{\bar{r}}\frac{\partial \bar{u}_c}{\partial \bar{r}}\right) - \bar{\sigma}\,\bar{B}_0^2\,\bar{u}_c - \frac{\bar{\mu}_c}{k}\,\bar{u}_c \tag{1}$$

$$\frac{\partial \bar{C}_c}{\partial \bar{t}} = \bar{D}_c\left(\frac{\partial^2 \bar{C}_c}{\partial \bar{r}^2} + \frac{1}{\bar{r}}\frac{\partial \bar{C}_c}{\partial \bar{r}}\right) - \bar{E}_c\,(\bar{C}_c - \bar{C}_0) \tag{2}$$

$$\bar{\rho}_c\,\bar{c}_c\,\frac{\partial \bar{T}_c}{\partial \bar{t}} = \bar{K}_c\left(\frac{\partial^2 \bar{T}_c}{\partial \bar{r}^2} + \frac{1}{\bar{r}}\frac{\partial \bar{T}_c}{\partial \bar{r}}\right) - \frac{\partial \bar{q}_c}{\partial \bar{r}} + \bar{Q}_c\,(\bar{T}_c - \bar{T}_0) \tag{3}$$

$$\bar{\rho}_p\,\frac{\partial \bar{u}_p}{\partial \bar{t}} = -\frac{\partial \bar{p}_p}{\partial \bar{z}} + \bar{\mu}_p\left(\frac{\partial^2 \bar{u}_p}{\partial \bar{r}^2} + \frac{1}{\bar{r}}\frac{\partial \bar{u}_p}{\partial \bar{r}}\right) - \bar{\sigma}\,\bar{B}_0^2\,\bar{u}_p - \frac{\bar{\mu}_p}{k}\,\bar{u}_c \tag{4}$$

$$\frac{\partial \bar{C}_p}{\partial \bar{t}} = \bar{D}_p\left(\frac{\partial^2 \bar{C}_p}{\partial \bar{r}^2} + \frac{1}{\bar{r}}\frac{\partial \bar{C}_p}{\partial \bar{r}}\right) - \bar{E}_p\,(\bar{C}_p - \bar{C}_0) \tag{5}$$

$$\bar{\rho}_p\,\bar{c}_p\,\frac{\partial \bar{T}_p}{\partial \bar{t}} = \bar{K}_p\left(\frac{\partial^2 \bar{T}_p}{\partial \bar{r}^2} + \frac{1}{\bar{r}}\frac{\partial \bar{T}_p}{\partial \bar{r}}\right) - \frac{\partial \bar{q}_p}{\partial \bar{r}} + \bar{Q}_p\,(\bar{T}_p - \bar{T}_0) \tag{6}$$

Where $\bar{\rho}_c, \bar{R}_c(\bar{z}), \bar{T}_c, \bar{c}_c, \bar{\mu}_c, \bar{u}_c, \bar{C}_c, \bar{K}_c, \frac{\partial \bar{q}_c}{\partial \bar{r}}, \bar{D}_c$, and $\bar{\alpha}_c$ are represented density, stenosis province, temperature profile, specific heat, viscosity, velocity profile, concentration profile, thermal conductivity, radiation effect, coefficient of mass diffusivity, and the mean radiation absorption respectively for core region, $\bar{\rho}_p$, $\bar{R}_p(\bar{z})$, $\bar{T}_p$, $\bar{c}_p$, $\bar{\mu}_p, \bar{u}_p$, $\bar{C}_p$, $\bar{K}_p$, $\frac{\partial \bar{q}_p}{\partial \bar{r}}$, $\bar{D}_p$, and $\bar{\alpha}_p$ are represented density, stenosis province, temperature profile, specific heat, viscosity, velocity profile, concentration profile, thermal conductivity, radiation effect, coefficient of mass diffusivity, and the mean radiation absorption respectively for plasma region and $\bar{B}_0, k, \bar{\sigma}$, are represented magnetic field intensity, permeability, electrical conductivity for both regions repectively

The following are the boundary conditions for decoding the concern problem for both partitions:

$$\left.\begin{aligned} &\bar{u}_p = 0,\ \bar{T}_p = \bar{T}_w,\ \bar{C}_p = \bar{C}_w \ \text{ at } \bar{r} = \bar{R}_p(\bar{z}) \\ &\bar{u}_c = \bar{u}_p,\ \bar{\tau}_c = \bar{\tau}_p,\ \bar{T}_p = \bar{T}_c,\ \frac{\partial \bar{T}_c}{\partial \bar{r}} = \frac{\partial \bar{T}_p}{\partial \bar{r}},\ \bar{C}_p = \bar{C}_c,\ \frac{\partial \bar{C}_c}{\partial \bar{r}} = \frac{\partial \bar{C}_p}{\partial \bar{r}} \ \ at\ \bar{r} = \bar{R}_c(\bar{z}) \\ &\frac{\partial \bar{T}_c}{\partial \bar{r}} = 0,\ \frac{\partial \bar{C}_c}{\partial \bar{r}} = 0,\ \frac{\partial \bar{u}_c}{\partial \bar{r}} = 0 \ \ at\ \bar{r} = 0 \end{aligned}\right\}$$

It is familiarizing the following dimensionless parameters.

$$r = \frac{\bar{r}}{\bar{R}_0}, t = \bar{t}\,\bar{w}, u_c = \frac{\bar{u}_c}{\bar{u}_0}, u_p = \frac{\bar{u}_p}{\bar{u}_0}, z = \frac{\bar{z}}{\bar{R}_0}, R_c(z) = \frac{\bar{R}_c(\bar{z})}{\bar{R}_0}, R_p(z) = \frac{\bar{R}_p(\bar{z})}{\bar{R}_0}\, \mu_0 = \frac{\bar{u}_p}{\bar{u}_c}, p_p = \frac{\bar{R}_0\,\bar{p}_p}{\bar{\mu}_p\,\bar{u}_0}, p_c = \frac{\bar{R}_0\,\bar{p}_c}{\bar{\mu}_p\,\bar{u}_0},$$
$$D_0 = \frac{\bar{D}_p}{\bar{D}_c}, \rho_0 = \frac{\bar{\rho}_p}{\bar{\rho}_c}, s_0 = \frac{\bar{c}_p}{\bar{c}_c}, \mathrm{R_e} = \frac{\bar{\rho}_p\,\bar{R}_0^2\,\bar{w}}{\bar{\mu}_p}, S_c = \frac{\bar{\mu}_p}{\bar{D}_p\,\bar{\rho}_p}, \theta_p = \frac{(\bar{T}_p - \bar{T}_0)}{(\bar{T}_w - \bar{T}_0)}, \theta_c = \frac{(\bar{T}_c - \bar{T}_0)}{(\bar{T}_w - \bar{T}_0)}, \sigma_c = \frac{(\bar{C}_c - \bar{C}_0)}{(\bar{C}_w - \bar{C}_0)}, \sigma_p =$$
$$\frac{(\bar{C}_p - \bar{C}_0)}{(\bar{C}_w - \bar{C}_0)}, M^2 = \frac{\bar{\sigma}\,\bar{B}_0^2\,\bar{R}_0^2}{\bar{\mu}_p}, N^2 = \frac{4\,\bar{\alpha}_p^2\,\bar{R}_0^2}{\bar{K}_p}, \mathrm{P_e} = \frac{\bar{c}_p\,\bar{\rho}_p\,\bar{R}_0^2\,\bar{w}}{\bar{K}_p}, K_0 = \frac{\bar{K}_p}{\bar{K}_c}, \alpha_0 = \frac{\bar{\alpha}_p^2}{\bar{\alpha}_c^2}, E_0 = \frac{\bar{E}_p}{\bar{E}_c}$$

Solution of the Problem

The pulsatile nature of blood circulation is taken into account when flow equations are used. We assume that the following are defined in dimensionless form as

$$u_c(r,t) = u_{c_0}(r)e^{iwt}, \sigma_c(r,t) = \sigma_{c_0}(r)e^{iwt}, \theta_c(r,t) = \theta_{c_0}(r)e^{iwt}, -\frac{\partial p_c}{\partial z} = P_0\,, u_p(r,t) = u_{p_0}(r)e^{iwt},$$
$$\sigma_p(r,t) = \sigma_{p_0}(r)e^{iwt}, \theta_p(r,t) = \theta_{p_0}(r)e^{iwt}, -\frac{\partial p_p}{\partial z} = P_0\, e^{iwt}$$

Equations (1) and (4) solve converting dimensionless form, and we obtained final solutions for both layers using dimensionless parameters and boundary conditions.

$$u_c(r,t) = \left\{C_1\, J_0(\varphi_c\, r) - \frac{F_c}{\varphi_c^2}\right\} e^{iwt} \text{ and } u_p(r,t) = \left\{C_3\, J_0\big(\varphi_p\, r\big) + C_4\, Y_0\big(\varphi_p\, r\big) - \frac{F_p}{\varphi_p^2}\right\} e^{iwt}$$

$$C_1 G_1 = \left[\varphi_p\, J_1(\varphi_p\, R_c)\big(Y_0(\varphi_p\, R_p)\, D_2 - Y_0(\varphi_p\, R_c)\, D_1\big) + \varphi_p\, Y_1(\varphi_p\, R_c)\big(J_0(\varphi_p\, R_c)D_1 - J_0(\varphi_p\, R_p)\, D_2\big)\right]$$

$$C_3 G_1 = \left[\varphi_C\, J_1(\varphi_C\, R_C)\big(Y_0(\varphi_p\, R_p)\, D_2 - Y_0(\varphi_p\, R_c)\, D_1\big) + \varphi_p\, Y_1(\varphi_p\, R_C)J_0(\varphi_C\, R_C)D_1\right]$$

$$C_4 G_1 = \left[\Big(\varphi_C\, J_1(\varphi_C\, R_C)J_0(\varphi_p\, R_C) - \varphi_p\, J_1(\varphi_p\, R_C)\, J_0(\varphi_C\, R_C)\Big)\, D_1 + \varphi_C\, J_1(\varphi_C\, R_C)J_0(\varphi_p\, R_p)\, D_2\right]$$

$$G_1 = \left[\Big(\varphi_C\, J_1(\varphi_C\, R_C)J_0(\varphi_p\, R_C) - \varphi_p\, J_1(\varphi_p\, R_C)J_0(\varphi_C\, R_C)\Big)\, Y_0(\varphi_p\, R_p) + G\, J_0(\varphi_p\, R_p)\right], D_2 = \frac{P_0}{\varphi_p^2} - \frac{P_0\mu_0}{\varphi_c^2}$$

$$D_1 = \frac{P_0}{\varphi_p^2}, G = \varphi_p\, Y_1(\varphi_p\, R_C)\, J_0(\varphi_C\, R_C) - \varphi_C\, J_1(\varphi_C\, R_C)Y_0(\varphi_p\, R_C)$$

Equations (2) – (7) solve converting dimensionless form, and we obtained final solutions for both layers using dimensionless parameters and boundary conditions.

$$\sigma_c(r,t) = C_5\, J_0(\psi_c\, r)\, e^{iwt} \quad \text{and} \quad \sigma_p(r,t) = \{C_7\, J_0(\psi_p\, r) + C_8\, Y_0(\psi_p\, r)\}\, e^{iwt}$$

$$C_5 G_2 = \left(\psi_p\, J_1(\psi_p\, R_C) Y_0(\psi_p\, R_C) - \psi_p\, Y_1(\psi_p\, R_C) J_0(\psi_p\, R_C)\right) e^{-iwt}$$

$$C_7 G_2 = \left(\psi_C\, J_1(\psi_C\, R_C) Y_0(\psi_p\, R_C) - \psi_p\, Y_1(\psi_p\, R_C) J_0(\psi_C\, R_C)\right) e^{-iwt}$$

$$C_8 G_2 = \left(\psi_p\, J_1(\psi_p\, R_C)\, J_0(\psi_C\, R_C) - \psi_C\, J_1(\psi_C\, R_C) J_0(\psi_p\, R_C)\right) e^{-iwt}$$

$$G_2 = \psi_C\, J_1(\psi_C\, R_C) \left(J_0(\psi_p\, R_p) Y_0(\psi_p\, R_C) - J_0(\psi_p\, R_C) Y_0(\psi_p\, R_p)\right) + \psi_p\, J_0(\psi_C\, R_C) \left(J_1(\psi_p\, R_C)\, Y_0(\psi_p\, R_p) - Y_1(\psi_p\, R_C)\, J_0(\psi_p\, R_p)\right)$$

Equations (2) – (7) solve converting dimensionless form, and we obtained final solutions for both layers using dimensionless parameters and boundary conditions.

$\theta_c(r,t) = C_9\, J_0(\lambda_c\, r)\, e^{iwt}$ and $\theta_p(r,t) = \{C_{11}\, J_0(\lambda_p\, r) + C_{12} Y_0(\lambda_p\, r)\}\, e^{iwt}$

$$C_9 G_3 = \left(\lambda_p\, J_1(\lambda_p\, R_C) Y_0(\lambda_p\, R_C) - \lambda_p\, Y_1(\lambda_p\, R_C) J_0(\lambda_p\, R_C)\right) e^{-iwt}$$

$$C_{11} G_3 = \left(\lambda_C\, J_1(\lambda_C\, R_C) Y_0(\lambda_p\, R_C) - \lambda_p\, Y_1(\lambda_p\, R_C)\, J_0(\lambda_C\, R_C)\right) e^{-iwt}$$

$$C_{12} G_3 = \left(\lambda_p\, J_1(\lambda_p\, R_C) J_0(\lambda_C\, R_C) - \lambda_C\, J_1(\lambda_C\, R_C) J_0(\lambda_p\, R_C)\right) e^{-iwt}$$

$$G_3 = \lambda_C\, J_1(\lambda_C\, R_C) \left(J_0(\lambda_p\, R_p) Y_0(\lambda_p\, R_C) - J_0(\lambda_p\, R_C)\, Y_0(\lambda_p\, R_p)\right) + \lambda_p\, J_0(\lambda_C\, R_C) \left(J_1(\lambda_p\, R_C)\, Y_0(\lambda_p\, R_p) - Y_1(\lambda_p\, R_C) J_0(\lambda_p\, R_p)\right)$$

The flow resistance λ and volumetric flow rate Q_c and Q_p are defined as

$$\lambda = \int_0^z \frac{P_0 e^{iwt}}{Q}\, dz,\; Q_p = 2\,\pi\, R_p^2 \int_{R_C}^{R_p} u_p(r,t)\; dr,\; Q_c = 2\,\pi\, R_p^2 \int_0^{R_c} u_c(r,t)\; dr$$

The total volumetric flow rate Q is calculated as $Q = Q_c + Q_p = \sum Q_l$

$$Q = 2\,\pi\, R_p^2\, B1_c\, e^{iwt} \int_0^{R_c} J_0(\varphi_c\, r)\; dr + 2\,\pi\, R_p^2\, B1_p\, e^{iwt} \int_{R_c}^{R_p} J_0(\varphi_p\, r)\; dr - \frac{2\,\pi\, P_0 \mu_0 R_p^2\, R_c e^{iwt}}{\varphi_c^2} + 2\,\pi\, R_p^2\, B2_p\, e^{iwt} \int_{R_c}^{R_p} Y_0(\varphi_p\, r)\; dr - \frac{2\,\pi\, P_0 R_p^2\, (R_p - R_c) e^{iwt}}{\varphi_p^2}$$

Result and Discussion

We conducted this study to learn the most important information about blood flow through the plasma and core layer. The Reynolds number, heat source, magnetic field parameter, Schmidt parameter, Peclet number, pressure gradient, radiation parameter, and chemical reaction are all used in this study to achieve an admirable effect. Also present in the plasma and core layers are thermal conductivity ratios, specific heat, viscosities, heat source, and mean radiation absorption coefficients. The default values of parameters used to evaluate the model's effectiveness are depicted graphically as as , $P_0 = 10$, $w = 1$, $\rho_0 = 1.05$, $\alpha_0 = 1$, $R_e = 0.9$, $\mu_0 = 1.02$, $M = 2$, $S_c = 0.5$, $N = 2$, $E = 0.7$, $P_e = 0.87$, $K_0 = 0.4$, $s_0 = 1$ $Rd_1 = 0.8$, $Rd_0 = 1$ [1,4, 13,18,19,20,25,26,30,31].

In figures 1–4, we want to look at how radiation parameters, Peclet number, pulse rate, and heat source affect the temperature profile in the constricted artery. Figure 1 depicts how the temperature profile of the core and plasma regions varies with the radiation parameter (N). The figure clearly shows that as the values of the radiation parameter increase, the temperature profile of the blood flow decreases. As a result, when plasma separates from red blood cells, as in two-phase analysis, the temperature profile in the core region is lower than in the plasma region due to the buoyancy force created by the radiation effect. Furthermore, with no radiation effect, the temperature profile exhibits exactly opposite behaviour for core and plasma regions, with higher values in the core region than in the plasma region. Figures 2 and 3 show temperature profiles with variations in Peclet number and pulse rate in the constricted artery. The temperature profile of both parameters (Peclet number and pulse rate) has the same trend as the radiation parameter. Figure 4 depicts the temperature account in the constricted artery with different values of a heat source parameter. According to the graph, increasing the heat source parameter causes the temperature to accelerate. Its beneficial effect on blood pressure and flow.

Figures (5–8) show the concentration profile in the constricted artery with the Reynold number, Schmidt number, chemical reaction, and pulse rate. Figures (5–8) show that increasing the Reynold number, Schmidt number, chemical reaction, and pulse rate individually decreases the concentration profile. All of the figures in the concentration account follow the same pattern. Figure 9 depicts the axial direction of flow resistance as a function of the magnetic field parameter. When there are positive changes in the magnetic field, the resistance flow curve through the magnetic field parameter reaches its maximum value. Figures (10-13) show the effect of several parameters on blood velocity in the stenotic artery, including the Reynolds number, magnetic field parameter, pressure gradient, and pulse rate. Figure 10 shows the change in velocity as well as the varying Reynolds number of the constricted artery. Because of the increase in the Reynold number, the blood velocity in the narrowed artery accelerates. In figure 11, the impact demonstrates the opposite change in velocity along with the varying magnetic field parameter of the stenosed artery when used with the magnetic field parameter on the velocity profile. In figure 12, increasing the pulse rate in the constricted artery causes the velocity profile to decrease, whereas increasing the pressure gradient causes the velocity profile to accelerate in figure 13.

Figure 14 depict the axial variation of shear stress on the outer and inner walls of the constricted artery in the presence of a magnetic field. Figure 14 depicts the effect of pressure gradient in the narrowed artery is accelerated.

Conclusion

We discussed developing a model to fill a research gap. As a result, the essential roles of the human physiological artery were investigated in relation to the heat source, chemical reaction, wall shear stress, magnetic field, radiation parameter, Reynold number, and Schmidt number. We discovered the critical flow parameters while working on the profiles, and if properly managed, they may be useful cardiovascular diseases.

• The treatment parameter, Reynold number, pressure gradient parameter, and heat source all have an effect on the axial velocity and temperature profile growth in our study.

• As the chemical reaction, pulse rate, peclet, Reynold, Schmidt, and magnetic field parameters increase, the concentration, temperature, and velocity profile decrease.

• Increasing the magnetic field parameter increases flow resistance and wall shear stress.

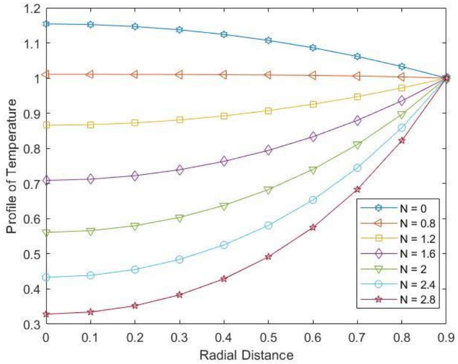

Fig. 1: Temperature Profile for specific entries of N along a radial distance

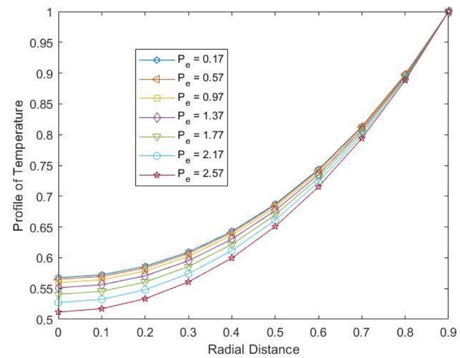

Fig. 2: Temperature Profile for specific entries of P_e are shown along a radial distance

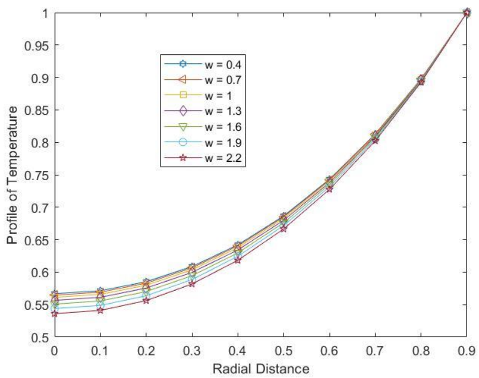

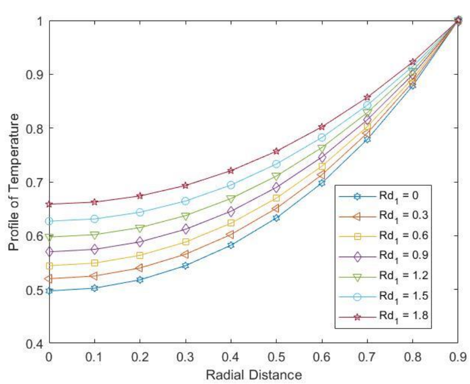

Fig. 3: Temperature Profile for specific entries of w are shown along a radial distance

Fig. 4: Temperature Profile for specific entries of Rd_1 are shown along a radial distance

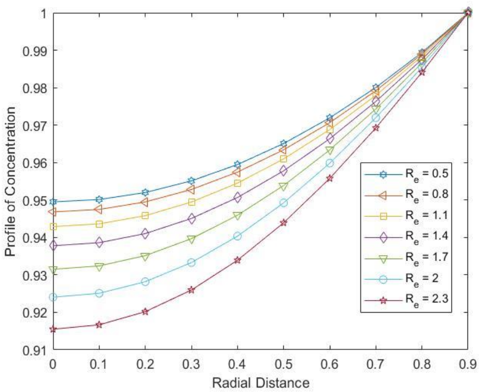

Fig. 5: Concentration Profile for specific entries of R_e are shown along a radial distance

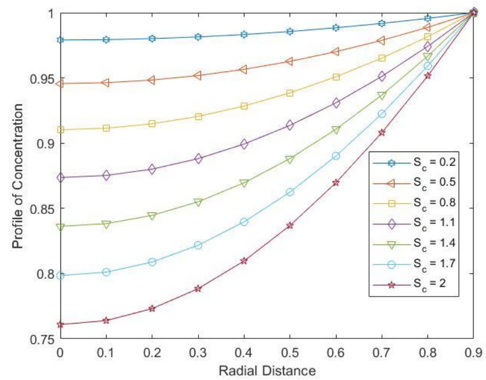

Fig. 6: Concentration Profile for specific entries of S_c are shown along a radial distance

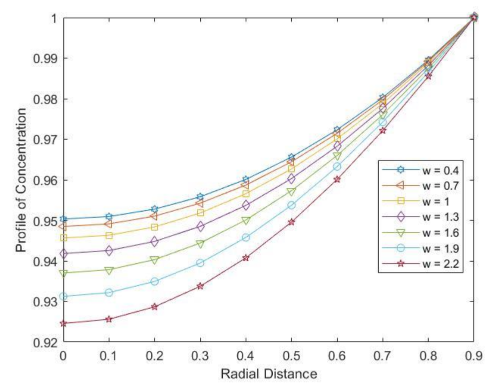

Fig. 8: Concentration Profile for specific entries of E are shown along a radial distance

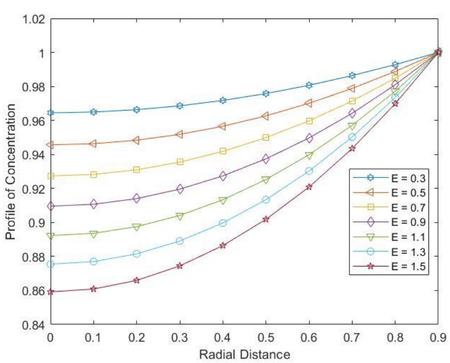

Fig. 7: Concentration Profile for specific entries of w are shown along a radial distance

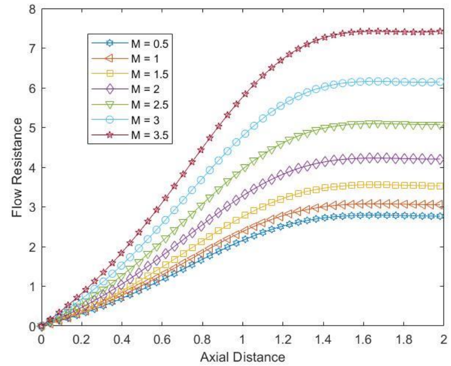

Fig. 9: Flow Resistance for specific entries of M are shown along an axial distance

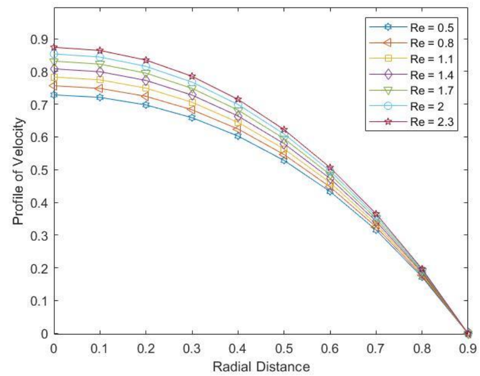

Fig. 10: Velocity Profile for specific entries of R_e are shown along a radial distance

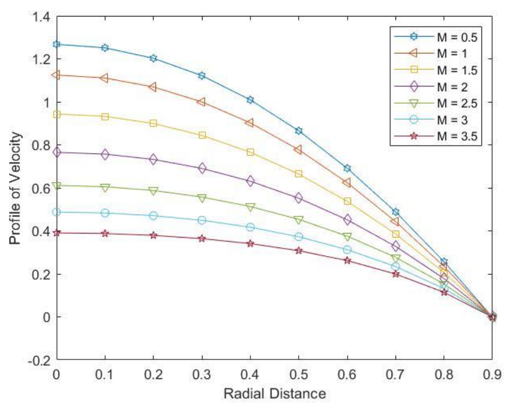

Fig. 11: Velocity Profile for specific entries of M are shown along a radial distance

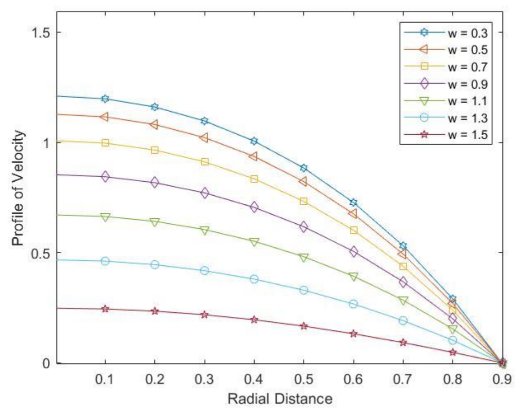

Fig. 12: Velocity Profile for specific entries of w are shown along a radial distance

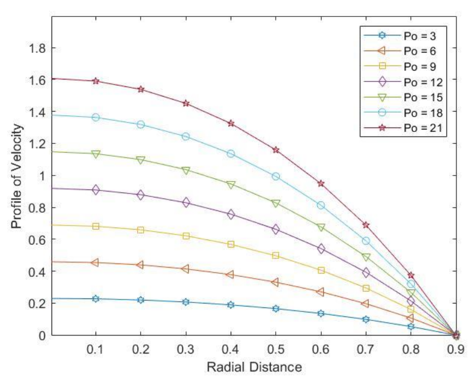

Fig. 13: Velocity Profile for specific entries of P_0 are shown along a radial distance

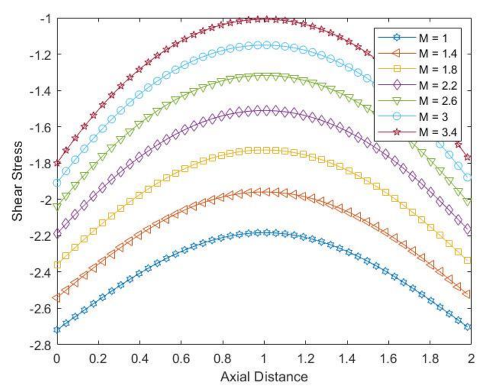

Fig. 14: Wall Shear Stress for specific entries of M are shown along an axial distance

References

1. R. Ponlagusamy and R. Manchi, A study on two-layered (K.L-Newtonian) model of blood flow in an artery with six types of mild stenosis,Appl. Math. Comput., 367 (2020) 1-22.
2. R. Ponalagusamy and R. Manchi, A four-layered model for flow of non-Newtonian fluid in an artery with mild stenosis, Sadhana, 44 (2019) 1-14.

3. K. M. Prasad, P. R. Yasa and J. C. Misra, Characteristics of blood flow through a porous tapered artery having a mild stenosis under the influence of an external magnetic field, J. Appl. Sci. and Eng., 24 (2021) 661-671.
4. B. Tripathi and B. K. Sharma, Two-phase analysis of blood flow through a stenosed artery with the effects of chemical reaction and radiation, Ric. di Mat. (2021) 1-27.
5. N. A. Shah, A. Al-Zubaidi and S. Saleem, Study of magnetohydrodynamic pulsatile blood flow through an inclined porous cylindrical tube with generalized time nonlocal shear stress, Adv. Math. Phy. 2021 (2021) 1-11.
6. R. Ponalagusamy and S. Priyadharshini, Couple stress fluid model for pulsatile flow of blood in a porous tapered arterial stenosis under magnetic field and periodic body acceleration, J. Mech. Medi. Biol. 17 (2017) 1750109-1-1750109-29.
7. R. Ponalagusamy, R. Priyadharshini and Pulsatile MHD flow of a Casson fluid through a porous bifurcated arterial stenosis under periodic body acceleration, Appl. Math. Comp. 333 (2018) 325-343.
8. R. Manchi and R. Ponalagusamy, Modeling of pulsatile EMHD flow of Aμ–blood in an inclined porous tapered atherosclerotic vessel under periodic body acceleration, Arch. Appl. Mech. 91 (2021) 3421-3447.
9. R. Padma, R. Ponalagusamy and R. Tamil Selvi, Mathematical modeling of electro hydrodynamic non-Newtonian fluid flow through tapered arterial stenosis with periodic body acceleration and applied magnetic field, Appl. Math. Comp. 362 (2019) 1-24.
10. J. U. Abubakar and A. D. Adeoye, Effects of radiative heat and magnetic field on blood flow in an inclined tapered stenosed porous artery, J. Taib. Uni. Sci. 14 (2020) 77-86.
11. M. S. Dada and F. A. Awoniran, Heat and mass transfer in micropolar model for blood flow through a stenotic tapered artery, Appli. Appl. Math. Int. J. 15 (2020) 1114-1134.
12. A. Jimoh, G. T. Okedayo and T. Aboiyar, Hematocrit and slip velocity influence on third grade blood flow and heat transfer through a stenosed artery, J. Appl. Math. Phy. 7 (2019) 638-663.
13. S. Sharma, U. Singh and V. K. Katiyar, Magnetic field effect on flow parameters of blood along with magnetic particles in a cylindrical tube, J. Magn. Magn. Mater. 377 (2015) 395-401.
14. A. Ali, A. Fatima, Z. Bukhari, H. Farooq and Z. Abbas, Non-Newtonian Casson pulsatile fluid flow influenced by Lorentz force in a porous channel with multiple constrictions: A numerical study, Korea-Aust. Rheol. J. 33 (2021) 79-90.
15. R. Abumandour, I. M. Eldesoky, M. Abumandour, K. Morsy and M. M. Ahmed, Magnetic field effects on thermal nanofluid flowing through vertical stenotic artery: Analytical study, Math. 10 (2022) 1-20.
16. K. W. Bunonyo, C. I. Cookey and E. Amos, Modeling of blood flow through stenosed artery with heat in the presence of magnetic field, Asia. Resea. J. Math. 8 (2018) 1-14.
17. R. Bali and U. Awsathi, A Casson fluid model for multiple stenosed artery in the presence of magnetic field, J. Sci. Tech. 3 (2012) 53-64.
18. D. Kumar, B. Satyanarayana, R. Kumar, S. Kumar and N. Deo, Application of heat source and chemical reaction in MHD blood flow through permeable bifurcated arteries with inclined magnetic field in tumor treatments, Resul. Appl. Math. 10 (2021) 1-13.
19. D. F. Jamil, R. Roslan, M. Abdulhameed and I. Hashim, Controlling the blood flow in the stenosed porous artery with magnetic field, SainsMalaysiana. 47 (2018) 2581-2587.
20. B. Tripathi and B. K. Sharma, Influence of heat and mass transfer on MHD two-phase blood flow with radiation, AIP Conf. Proceed. 1975 (2018) 030009-1-030009-8.
21. S. Kumar and S. Kumar, Blood flow through an elliptical stenosed artery with the heat source and chemical reaction, Res. J. Biotech. 17(12) (2022) 82-90.
22. Manisha and S. Kumar, Effect of cosine shape stenosis on non-Newtonian blood flow with casson model in stenosed artery, IJETT, 70(8) (2022) 336-346.
23. R. Abumandour, I. M. Eldesoky, M. Abumandour, K. Morsy and M. M. Ahmed, Magnetic field effects on thermal nanofluid flowing through vertical stenotic artery: Analytical study, Mathematics,10(492) (2022) 1-20.

24. J. Awrejcewicz, A. A. Zafar, G. Kudra and M. B. Riaz, Theoretical study of the blood flow in arteries in the presence of magnetic particles and under periodic body acceleration, Chaos Solitons Fractals, 140 (2020) 1-12.
25. K. W. Bunonyo and I.C. Eli, Oscillatory flow of LDL-C and blood fluid through a slanted channel with heat within the sight of magnetic field, EJ-Physics, 5(3) (2021) 37-44.
26. C. Kumawat, B. K. Sharma, Q. M. Al-Mdallal and M. R. Gorji, Entropy generation for MHD two phase blood flow through a curved permeable artery having variable viscosity with heat and mass transfer, Int. Commun. Heat Mass Transf., 133 (2022) 1-23,
27. S. Majeed, F. Ali, A. Imtiaz, I. Khan and M. Andualem, Fractional model of MHD blood flow in a cylindrical tube containing magnetic particles,Sci. Rep., 12 (2022) 1-16.
28. R. Padma, S. R. Tamil and R. Ponalagusamy, Analysis of MHD pulsatile flow of Jeffrey fluid in a diseased inclined tapered porous artery exposed to an inclined magnetic field, J. Phys.: Conf. Ser., 1850 (2021) 1-14.
29. Poonam, B. K. Sharma, C. Kumawat and K. Vafai, Computational biomedical simulations of hybrid nanoparticles (Au-Al_2O_3/ blood-mediated) transport in a stenosed and aneurysmal curved artery with heat and mass transfer: hematocrit dependent viscosity approach, Chem. Phys. Lett., 800 (2022) 1-22.
30. M. Sharma, B. K. Sharma, R. K. Gaur and B. Tripathi, Soret and Dufour effects in biomagnetic fluid of blood flow through a tapered porous stenosed artery, J. Nanofluids, 8 (2019) 327-336.
31. S. U. Siddiqui, S. R. Shah and Geeta, A biomechanical approach to study the effect of body acceleration and slip velocity through stenotic artery, Appl. Math. Comput., 261 (2015) 148-155.